Dynamic Duo: Design and Validation of an Autonomous Frontal and Sagittal Actuating Hip Exoskeleton for Balance Modulation During Perturbed Locomotion

Jennifer K. Leestma, *Graduate Student Member, IEEE*, Snehil Mathur, Maximilian D. Anderton, Gregory S. Sawicki, *Member, IEEE*, and Aaron J. Young, *Senior Member, IEEE*

***Abstract*—Humans are required to maintain balance during locomotion in challenging environments, which present an even bigger challenge for individuals with balance impairments. Exoskeleton-driven balance augmentation is a promising avenue to assist users in these environments, but there has been little work in developing exoskeleton devices for these applications. In this work, we present the design, realization, and validation of an autonomous robotic hip exoskeleton with frontal and sagittal actuation. This device contains four quasi-direct drive-actuated degrees of freedom, enabling both frontal and sagittal assistance at the hip joints. The device is relatively light-weight, weighing 7.76 kg, and low-profile in the frontal plane, enabling unimpeded arm swing of the user. We found that wearing the device did not change walking kinematics, validating that the design does not inhibit the user's natural motion. We validated the exoskeleton using a bilateral bang-bang controller that successfully modulated step width and length in all cardinal and ordinal directions (all $p<0.001$) during steady state and perturbed walking. We also found that step modulation capability is influenced by swing leg kinematics and perturbation context. Broadly, this work presents a lightweight, autonomous, powered exoskeleton that can be used to study control approaches for balance augmentation.**

Manuscript received 26 October 2023; accepted 7 February 2024. Date of publication 28 February 2024; date of current version 19 March 2024. This letter was recommended for publication by Associate Editor V. Vashista and Editor P. Valdastri upon evaluation of the reviewers' comments. This work was supported in part by the National Science Foundation Graduate Research Fellowship Award 1324585, in part by the National Science Foundation Research Traineeship Award 1545287, and in part by the National Institutes of Health Director's New Innovator Award DP2-HD111709. *(Corresponding author: Jennifer K. Leestma.)*

This work involved human subjects or animals in its research. Approval of all ethical and experimental procedures and protocols was granted by Georgia Institute of Technology Institutional Review Board under Application No. H21076.

Jennifer K. Leestma and Aaron J. Young are with the Institute for Robotics and Intelligent Machines, Georgia Institute of Technology, Atlanta, GA 30332 USA, and also with the Woodruff School of Mechanical Engineering, Georgia Institute of Technology, Atlanta, GA 30332 USA (e-mail: jleestma@gatech.edu).

Snehil Mathur is with the School of Electrical and Computer Engineering, Georgia Institute of Technology, Atlanta, GA 30332 USA.

Maximilian D. Anderton is with the Woodruff School of Mechanical Engineering, Georgia Institute of Technology, Atlanta, GA 30332 USA.

Gregory S. Sawicki is with the Institute for Robotics and Intelligent Machines, Georgia Institute of Technology, Atlanta, GA 30332 USA, also with the Woodruff School of Mechanical Engineering, Georgia Institute of Technology, Atlanta, GA 30332 USA, and also with the School of Biological Sciences, Georgia Institute of Technology, Atlanta, GA 30332 USA.

Digital Object Identifier 10.1109/LRA.2024.3371290

***Index Terms*—Wearable robotics, prosthetics and exoskeletons, physically assistive devices.**

I. Introduction

MAINTAINING sagittal and frontal stability is required for bipedal locomotion [1]. However, traversing daily perturbations, such as curbs, patches of ice, or getting bumped by a stranger on the bus, can challenge our ability to maintain stable gait. These perturbations are more challenging for individuals with balance impairments and are more likely to cause falls, which can be detrimental to the health and independence of these individuals [2], [3].

Various types of wearable robots, spanning exoskeletons to wearable gyroscopes, have the ability to improve stability and aid in balance recovery by providing assistance to a user [4], [5], [6], [7], [8]. However, the majority of wearable robotics research has focused on exoskeletons targeting other objectives, notably metabolic cost augmentation during steady state locomotion and injury reduction in manual labor tasks. Though this research has driven a surge in exoskeleton development, few devices have been designed or evaluated for augmentation of balance during locomotion [4], [9], [10].

For healthy or partially impaired individuals, current work supports the use of single-joint exoskeletons that allow for shared control between the user and device, in contrast to full lower limb exoskeletons that independently control a user's motion. When evaluating which lower limb joint should be the targeted for balance augmentation, we look to biomechanics literature that has investigated the role of lower limb joints in balance recovery. The hip and ankle are the primary contributors to balance-correcting recovery strategies. Ankle-based strategies provide constant, but small, shifts of the center of pressure under the foot [11]. However, these strategies primarily contribute in the sagittal plane due to the significantly longer moment arm along the foot in that direction, limiting the effectiveness of this strategy for lateral balance regulation. In contrast, hip-based strategies drive changes in step placement that enable large, abrupt changes to the center of pressure at the end of each step in both the mediolateral and anteroposterior directions [11], [12]. This step placement modulation is key for correcting large amounts of instability in both the frontal and sagittal planes, indicating that hip-centered exoskeleton assistance may be a more important to combat fall-inducing perturbations [13]. However,

2377-3766 © 2024 IEEE. Personal use is permitted, but republication/redistribution requires IEEE permission.
See https://www.ieee.org/publications/rights/index.html for more information.

Authorized licensed use limited to: Georgia Institute of Technology. Downloaded on January 06,2025 at 23:11:39 UTC from IEEE Xplore. Restrictions apply.

hip exoskeleton research has primarily focused on devices with a single sagittal degree of freedom, with few designs featuring frontal plane actuation [14]. Additionally, added mass has been shown to affect kinematic stability by altering limb inertia [15]. Distally added mass may have an increased impact on stability by increasing momentum about the center of mass (COM), suggesting that proximally added mass is more favorable, again suggesting the hip as the ideal joint to assist [16]. Due to the importance of stepping strategy and lessened impact of added mass, we propose that an exoskeleton with frontal and sagittal actuation at the hip is a "dynamic duo" that is the best suited for balance augmentation and fall prevention.

An ideal device for this application would be (1) low-profile and lightweight, to enable natural kinematics and limit the effect of added mass, (2), fast-acting, to enable rapid responses to loss of balance, and (3) provide sufficient torque for balance recovery, while avoiding unnecessarily high torque capabilities that may increase actuator mass or decrease velocity and backdrivability. Only a handful of sagittal and frontal actuating hip exoskeletons have been developed [4], [9], [10], [17]. All of these devices have a worn mass that exceeds 9 kg, which could adversely affect body segment inertia and balance outcomes [16]. Some designs incorporated solutions to enable natural arm swing, which is crucial for transverse stabilization and limiting biomechanical effects of wearing a device [9], [16], [18], [19]. Some of the previously developed systems are capable of high torques, achieved through higher gear ratios, which could inhibit sufficiently fast responses during perturbed walking trials [4]. Though these designs present impressive torque capabilities, all exceeding 50 Nm, it is unclear if this level of assistance is needed for balance applications and step placement modification [4], [9]. Incorporating biomechanical data from target use-cases could help refine actuator specifications, enabling sufficient assistive torque while limiting added mass and enhancing speed and backdrivability.

Here, we present our first-generation design, realization, and the preliminary validation of an autonomous sagittal and frontal actuating hip exoskeleton for balance modulation. Our device uses quasi-direct drive (QDD) actuators, which enable high speeds and backdrivability and were selected based on human kinematic and kinetic data during steady state and perturbed walking. The total worn weight of the device is 7.2 kg (this includes batteries, microprocessor, and all electronics) and the lateral low-profile enables natural arm swing. To preliminarily validate the capabilities of the device, we designed a bang-bang-style controller that applies bilateral assistance during the single stance phase of walking (i.e., torque applied to both stance and swing legs during this time) to drive step placement in various directions. We found that the exoskeleton is able to successfully and mechanistically modulate step placement in both steady state and perturbed walking. Additionally, we found that the step placement modulation capability of the device changes with the direction of exoskeleton assistance and whether or not the user is walking in a perturbed context.

II. Hip Exoskeleton Design

Here, we present the mechanical, interface, electronic, and controller design for a sagittal and frontal actuating hip exoskeleton. Our device can be adjusted to fit a large portion of the general population, spanning a 25th percentile female to a 95th percentile male [20]. The total device weight is lighter than previously published sagittal and frontal actuating devices, weighing 7.30 kg without batteries and 7.76 kg with single battery operation. We designed the exoskeleton to have a discreet profile, protruding only 6.5 cm laterally in the area where users' arms naturally swing, enabling them to maintain a natural arm motion. Additionally, we used QDD actuators, providing high backdrivability and speed. Because the intended operation of the exoskeleton is in balance-modulation contexts, we informed actuator selection and device range of motion capabilities using both steady state and perturbed walking data during a large variety of perturbations [12], [21].

A. Actuator Selection

We began by evaluating commercially available QDD actuators (gear ratio at or below 12:1). QDD actuators are highly backdrivable due to low reflected inertia, are capable of high speeds, and enable high-precision current control. These characteristics make QDD actuators excellent candidates for wearable robots and have been previously validated and discussed for these applications [22]. We considered the T-Motor AK60-6, AK80-6, AK80-9, AK70-10, AK80-8, and AK10-9, as these were some of the most suitable QDD actuators for our application. These actuators enable open-loop torque control from a user implementation standpoint due to precise closed-loop current control on the native motor drivers.

The target use case of our exoskeleton is for balance augmentation using bio-inspired torque controllers. Therefore, we sought to evaluate the ability of each actuator to apply some percentage of biological torque across a variety of destabilizing environments. Our target biological torque percentage was set at 20%; there is relatively little work that has investigated optimal torque magnitudes for balance applications so we set this target percentage based on previous work that studied the optimal sagittal hip torque for energetic cost reduction [23].

To evaluate each actuator, we used our previously published data set of perturbed walking [12]. This data set contained 96 different perturbed walking conditions and we used data for a representative 80 kg participant. From this data, we used flexion/extension and ad/abduction hip moments during both steady state and perturbed walking, with the latter including three repetitions of each of the 96 perturbation conditions.

For each actuator, we performed the following analysis using the actuator voltage (V_{act}), motor torque (τ_{act}), motor resistance (R_{act}), torque constant (K_T), and actuator angular velocity (ω_{act}). We defined the required voltage from the actuator using:

$$V_{\text{act}} = \frac{\tau_{\text{act}} * R_{\text{act}}}{K_T} + K_T * \omega_{\text{act}} \tag{1}$$

where the actuator's angular velocity was defined using the biological angular velocity (ω_{hip}) and actuator gear ratio ($C_{\text{gear ratio}}$):

$$\omega_{\text{act}} = \omega_{\text{hip}} * C_{\text{gear ratio}} \tag{2}$$

and the required actuator torque was defined using the biological hip moment (M_{hip}) and some biological torque percentage ($C_{\text{percent bio}}$):

$$\tau_{\text{act}} = M_{\text{hip}} * C_{\text{percent bio}} \tag{3}$$

We determined the maximum biological torque percentage that each actuator was capable of that satisfied the following conditions: 1) the rated voltage of the actuator was not exceeded,

Authorized licensed use limited to: Georgia Institute of Technology. Downloaded on January 06,2025 at 23:11:39 UTC from IEEE Xplore. Restrictions apply.

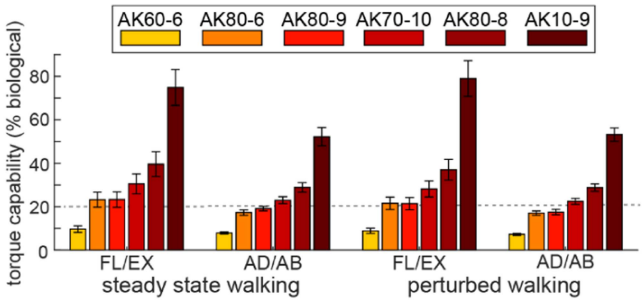

Fig. 1. Actuator analysis shows the capability of each actuator, as a percentage of biological torque, assuming continuous operation. The grey dashed line show the target 20% biological torque capability.

2) the peak assistive torque did not exceed the actuator's peak torque, and 3) the root mean squared (RMS) assistive torque did not exceed the actuator's rated torque. We did not consider actuator velocity due to the velocity limits of our candidate actuators greatly exceeding the hip joint velocities seen during perturbed walking [12], [24].

Using this framework, we determined the peak biological torque capability, as a percentage, for each actuator (Fig. 1). The two actuators that best matched the desired 20% biological torque target were the AK80-6 and AK80-9. Because the rated and peak torques of the AK80-9 were slightly higher, by 3 Nm and 6 Nm, respectively, and there was no weight difference between the models, we chose the AK80-9 for our device.

B. Mechanical Design

We designed our exoskeleton with the frontal and sagittal plane actuators in series; the sagittal plane actuator is mounted to the output shaft of the frontal actuator. The frontal actuators sit posteriorly to the hips, providing adduction/abduction assistance. They are permanently fixed 178.4 mm apart, based on the mean anatomical distance between the femoral heads [25]. Because this distance only has a standard deviation of $\pm$11.4 mm, which is well within the bounds of hip joint center estimations using non-invasive methods [26], we designed an actuator mount that holds both frontal actuators at this fixed distance (Fig. 2, shown in green). This mount is also discretely adjustable in the vertical direction to enable proximodistal centering of the actuators on the hip joints. Based on steady state and perturbed walking data, the frontal plane range of motion was designed to accommodate up to 25° of hip adduction and 30° of hip abduction, which is constrained with a mechanical hard stop [12], [21].

The sagittal actuators are connected through a series of aluminum rods at a perpendicular configuration relative to the ipsilateral frontal actuator. The aluminum rod frame and corner junctions were modeled after a previously published, publicly available design due to the ease of fabrication, rigidity, low weight, and previous validation [9]. We modified the rods and corresponding connections to have a D-profile, ensuring perpendicular and horizontal configuration of the sagittal actuators relative to the frontal actuators. We designed a sagittal actuator mount that is mounted to the lateral aluminum rod (Fig. 2, shown in blue). All actuator mounts were fabricated using aluminum 7075-T6 due to its low weight and high specific strength. Again, based on steady state and perturbed walking data, the sagittal plane range of motion was designed to accommodate up to 75° of hip flexion and 35° of hip extension, with mechanical hard stops at 96° and 78°, respectively, allowing more extensive range of motion than is necessary for this task [12], [21].

C. Interface Design

We designed torso and thigh interfaces to support the actuators at the hips. The main structure of the torso interface is a commercially available back brace (Optec USA, Georgia, USA) with added aluminum and steel components replicated from a publicly available design [9] that enables better distribution of exoskeleton mass vertically across the brace. The frontal actuator mount, mentioned previously, is attached directly to the aluminum components on the torso interface.

The actuator output shaft is attached to the thigh interface using custom aluminum and carbon fiber struts. For safety purposes, the actuator output shaft's safety factor was designed such that it would be the first component to fail, which would then inhibit the actuators from transmitting torque to the user. The thigh strut is a 3D-printed carbon fiber-reinforced nylon composite strut with a single longitudinal corrugation to increase stiffness and resist bending. We reinforced the struts with unidirectional carbon fiber tape layered with resin (Fig. 2, shown in purple). The proximal end of the thigh strut is attached to the output shaft connector as well as an upper thigh strap guide (Fig. 2, shown in yellow).

The base of the thigh interface is a piece of 4.75 mm thick Rolyan thermoplastic splinting material (Performance Health, Illinois, USA) that was thermoformed to mimic the curvature of the thigh (Fig. 2, shown in white). This cuff is somewhat flexible, allowing the material to bend and fit users' thigh circumferences. In parallel with this cuff is a 3D printed piece that provides fixed points for straps that wrap around the thigh cuff (Fig. 2, shown in black). Both the thigh cuff and the cuff strap piece attach to the distal end of the carbon fiber thigh strut.

D. Mechatronic Design

The central hub of the mechatronics system is a Jetson Orin Nano (NVIDIA, California, USA), which we chose due to its state-of-the-art computational speeds and native CAN communication ability, enabling direct communication with the actuators (Fig. 3). Each of the actuators communicates with the Jetson Orin Nano via a CAN transceiver board (Waveshare Electronics, Shenzhen, China). We also incorporated four force-sensitive resistors (FSRs; Adafruit, New York, USA) to act as foot switches, providing gait event information to the exoskeleton, via the Jetson's general-purpose input/output (GPIO) pins. The GPIO pins are also configured to receive trigger signals from external equipment to enable data synchronization and other information from our perturbation system, which is the target use case for this device. The mechatronics system is powered using a 24 V 2.0 Ah lithium ion drill battery (Kobalt, North Carolina, USA); one or two batteries can be used in our design, with the latter option being included for longer duration experiments and hot-swapping.

E. Gravity Compensation Controller

Due to the in-series layout of the frontal and sagittal plane actuators, we implemented gravity compensation to prevent undesired forces being applied to the user and preventing distal movement of the thigh interface over time. The weight of the connector bars, sagittal actuator, and leg interface cause an adduction moment about the frontal plane actuator. This results

Authorized licensed use limited to: Georgia Institute of Technology. Downloaded on January 06,2025 at 23:11:39 UTC from IEEE Xplore. Restrictions apply.

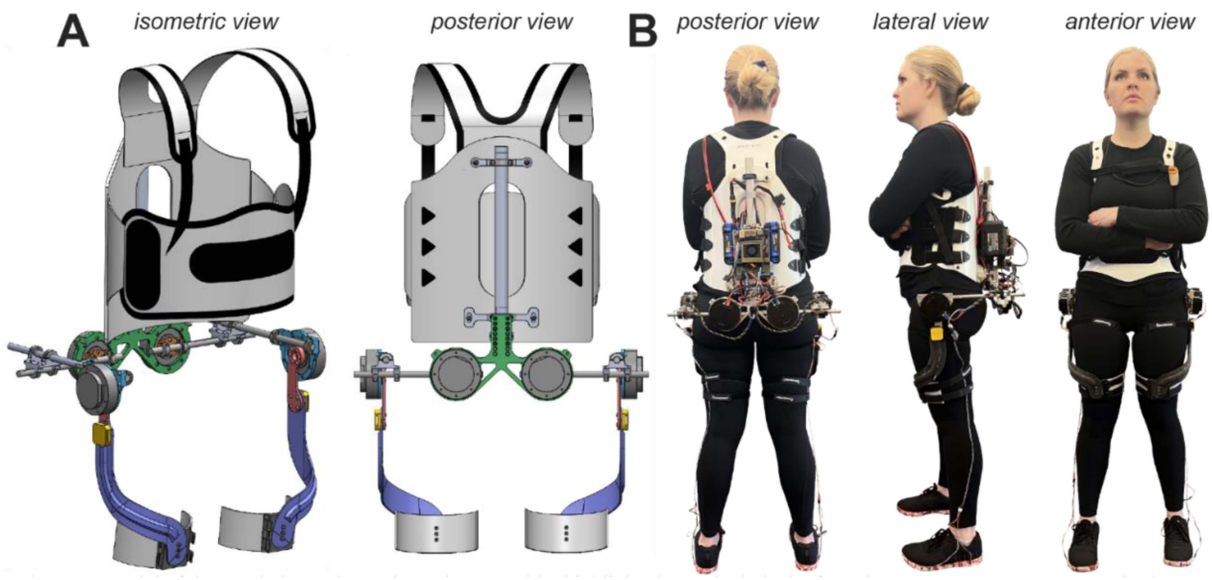

Fig. 2. (a) CAD model of the exoskeleton shows the entire assembly; highlighted parts include the frontal actuator mounts (green), sagittal actuator mounts (blue), actuator output shaft attachments (red), upper thigh strap guide (yellow), and carbon fiber thigh strut (purple). (b) Multiple views of the fabricated and worn exoskeleton, including mechatronics setup on the back.

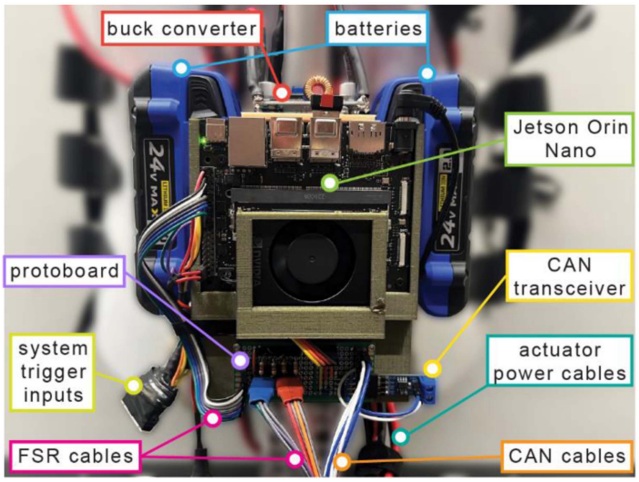

Fig. 3. Exoskeleton's mechatronics is powered by two lithium-ion drill batteries. The Jetson Orin Nano communicates with the actuators via a CAN transceiver, while also receiving peripheral sensors and external triggers.

in a medial force being applied to the user's leg, which could induce a narrower step width or the need for additional abductor muscle activation to maintain typical step width. To eliminate the influence of component mass on the user, we implemented a gravity compensation algorithm for the frontal actuators. Our approach assumed that the user's torso remained in vertical alignment with the global frame and static actuator orientation (i.e., instantaneous positions in time were incorporated, velocities and accelerations were not). We defined the following transformation matrices for the system:

$$ {}^{0}T_{1} = \begin{bmatrix} \cos\theta_f & -\sin\theta_f & 0 & 0 \\ \sin\theta_f & \cos\theta_f & 0 & 0 \\ 0 & 0 & 1 & 0 \\ 0 & 0 & 0 & 1 \end{bmatrix} \tag{4} $$

$$ {}^{1}T_{2} = \begin{bmatrix} \cos\theta_s & -\sin\theta_s & 0 & 0 \\ 0 & 0 & -1 & a_{ML} \\ \sin\theta_s & \cos\theta_s & 1 & -d_{AP} \\ 0 & 0 & 0 & 1 \end{bmatrix} \tag{5} $$

where d_{ML} and d_{AP} are scalar values that change as the interface is fit to each user's hip width and depth, respectively, θ_f is the frontal actuator angle, and θ_s is the sagittal actuator angle (Fig. 4). We obtained these angle measurements using the encoders that are natively incorporated into the exoskeleton's T-Motor AK80-9 actuators. Each actuator angle is relative to a "zeroed angle" taken while the participant stood in a neutral position with feet shoulder-width apart.

To simplify the gravity compensation calculations, we grouped the system into eight sets of components – 1) frontal plane bar, 2) corner connector, 3) sagittal plane bar, 4) sagittal actuator, 5) sagittal actuator mount, 6) sagittal output shaft connector, 7) thigh strut, and 8) distal thigh interface. For each group, associated fasteners, straps, and small 3D printed parts were included in group weight. However, we only considered the named component when defining the group's COM location, which was determined using the CAD model. The COM for groups 1–5 were defined in coordinate frame 1 while groups 6–8 were defined in coordinate frame 2 (Fig. 4). We used the transformation matrices to calculate the COM positions about the frontal plane output shaft, which was then used to calculate the instantaneous moment about the actuator caused by the weight of the components. When the exoskeleton is adjusted to fit the smallest and largest possible users, the maximum required gravity compensation torque across the exoskeleton's range of motion is 1.15 and 3.21 Nm, respectively. We incorporated this information into a controller that applied an equal and opposite torques to the frontal actuators to combat system weight, while commanding zero torque to the sagittal actuators; we updated these torques at 200 Hz. Throughout pilot testing, the addition of the gravity compensation controller significantly improved user

Authorized licensed use limited to: Georgia Institute of Technology. Downloaded on January 06,2025 at 23:11:39 UTC from IEEE Xplore. Restrictions apply.

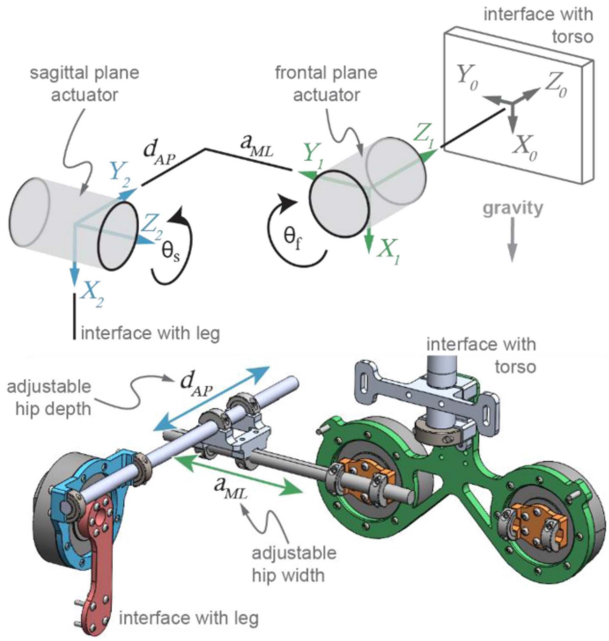

Fig. 4. Exoskeleton kinematic layout consists of reference frames centered about the frontal (frame 1) and sagittal (frame 2) axes of rotation. Constants d_{AP} and a_{ML} are based on participant-specific measurements after fitting. This layout was used to determine the rotation matrices for gravity compensation about the frontal actuators, where a compensation torque is applied about θ_f.

comfort by supporting the device's weight and inhibiting distal movement of the thigh struts over time during use.

F. Control Algorithm

The goal of our initial controller is to provide a burst of torque during the single stance phase of walking to characterize the step placement modulation capabilities of the exoskeleton. We designed a bang-bang controller that applied torque to the stance and swing limbs (Fig. 5(c)). For this controller to mimic physiologically realistic bilateral torques, we analyzed the single stance phase frontal and sagittal plane hip torques during perturbed walking from a previous data set [12]. We found that, across a diverse set of destabilizing scenarios, the ratio of stance to swing limb peak torque was approximately 2:1. We used this to scale the magnitude of the control signal, with swing limb magnitude being half that of stance limb magnitude.

We designed eight different assistance profiles that were intended to cause a variety of step placement deviations; the torque profiles are designed to cause some directional movement of the foot, which is the end effector of the leg segment being actuated at the hip joint. This included eight conditions, spanning medial (i.e., narrower step), lateral (i.e., wider step), anterior (i.e., longer step), posterior (i.e., shorter step), and the four corresponding ordinal diagonals (Fig. 5(b)). We applied differential torques to the stance and swing limb, where limb torque directions are mirrored to provide constructive assistance towards the same step placement deviation direction (Fig. 5(d)). We limited the controller's peak torque to 12 Nm; with the actuators' 18 Nm torque limit, pilot results that show very transient overshoot up to 2.5 Nm proceeding torque onset of the bang-bang controller, and gravity compensation able to reach a maximum of 3.21 Nm dependent on configuration, 12 Nm was set as a conservative safety limit. As stated previously, the combined frontal and sagittal magnitude of swing limb assistance was half of the stance limb assistance. Thus, we set these values to 6 Nm and 12 Nm for the swing and stance limbs, respectively.

To identify the single stance phase of walking, we used FSRs on the underside of the heel and toe of both feet; these high/low signals enabled us to identify when each heel and toe contacts the ground, thus enabling us to identify stance and swing phases. The controller parameters for each trial included the target swing leg and exoskeleton assistance condition. It is configured to wait for an external trigger and then apply assistance during the proceeding swing phase. For perturbed walking trials, this trigger is sent to the exoskeleton at the perturbation onset from the controller for the perturbation platform. For steady state walking trials, the FSRs were used to identify the start of swing phase, which initiates the assistance. For all trials, assistance ended at the end of single stance phase, which we also identified using the FSRs (Fig. 5(c)).

III. Human Subject Testing

A. Experimental Design

One healthy adult (female, 21 years old, 71.5 kg) participated in this study approved by the Georgia Institute of Technology Institutional Review Board. The participant had not previously worn the exoskeleton or participated in a perturbation study. We began by fitting the participant with the exoskeleton; in addition to wearing the device, the participant's shoe soles were instrumented with FSRs beneath the heel and fifth metatarsal joint. The participant walked at 1.25 m/s on an instrumental treadmill mounted in a Stewart platform (CAREN, Motek Medical, Netherlands), which enabled perturbations via surface translations (Fig. 5(a)). We collected motion capture data of a 22-marker lower limb marker set at 100 Hz. We collected actuator encoder position, actuator torque, and FSR data from the exoskeleton at 200 Hz. Both acquisition system's data was synchronized using a trigger that we generated using the perturbation system's controller.

The two sections of the experiment consisted of steady state and perturbed trials. In each of these sections, we collected ten exoskeleton conditions; these conditions included walking without the exoskeleton (no exo), walking while wearing the exoskeleton with only gravity compensation torques (no assist), and the eight exoskeleton assistance conditions (Fig. 5(b)).

For the steady state section, we collected one-minute trials for the no exo and no assist conditions. For the exoskeleton assisted portion, the participant walked while being exposed to one assistance condition approximately every 15 seconds, with the exact timing being pseudo-randomized. Each of the eight exoskeleton assistance conditions was applied five times per leg in a randomized order, leading to 80 steady state trials.

For the perturbed section of the experiment, we used a single perturbation condition from a surface translation experimental protocol that we previously developed and validated [12]. The perturbation caused the walking surface to slide diagonally – laterally and posteriorly – relative to the participant's leading stance leg. This typically causes a medial and anterior pitch of the participant's COM. This perturbation was applied at the end of the double stance phase of walking, which was identified

Authorized licensed use limited to: Georgia Institute of Technology. Downloaded on January 06,2025 at 23:11:39 UTC from IEEE Xplore. Restrictions apply.

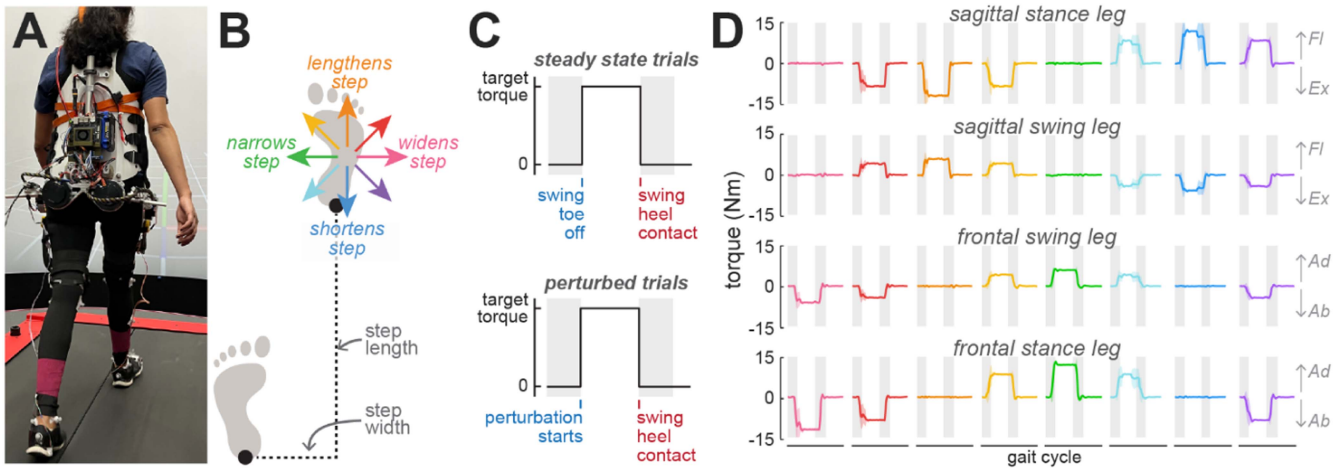

Fig. 5. (a) One participant walked at 1.25 m/s at steady state and while being exposed to a diagonal ground translation perturbation. (b) Eight exoskeleton conditions were applied to modulate user step placement, producing the colored exoskeleton assistance vectors which represent the expected foot placement deviation in the transverse plane. (c) The bang-bang controller is initiated by the release of the target swing toe switch (steady state trials) indicating or perturbation trigger (perturbed trials) and ended by the press of the target swing heel switch. (d) Each condition was applied during single stance phase using torque profiles from the four actuators. The grey and white backgrounds indicate double and single stance, respectively. Sagittal graphs show flexion (+) and extension (−) torques while frontal graphs show adduction (+) and abduction (−) torques. Note that the frontal plane assistance in the same direction graphically is opposite in direction in the global frame; for example, abduction assistance (negative on graph) causes outward rotation for both legs, which is a mirrored movement in the global frame.

using a real-time motion capture marker-based kinematic gait event detection method explained in detail in [12]. We collected five perturbation trials per leg for the no exo, no assist, and eight assistance conditions, leading to ten repetitions for each condition. All experimental timing and randomization were the same as previously stated.

B. Experimental Data Processing

We evaluated step width and length as the mediolateral and anteroposterior distance between the heel markers, respectively. For the steady state trials without exoskeleton assistance, we evaluated the last ten steps of the one-minute trials. For perturbed and exoskeleton assisted trials, we evaluated step placement at the end of the target single stance phase. The target single stance phase for steady state trials was the one in which exoskeleton assistance was provided. The target single stance phase for the perturbed trials was the single stance immediately following perturbation onset. We discarded trials if exoskeleton torque did not onset in the first 25% of single stance, which could occur due to errors in the experimental system's real-time gait cycle tracking or in the FSR trigger signals.

We also evaluated how the angle between the direction of the exoskeleton assistance vector, which we defined as the expected foot placement deviation in the transverse plane due to the exoskeleton assistance condition (Fig. 5(c)), relative to the direction of the swing limb influenced changes in step placement; the swing limb direction was defined by the velocity vector in the last 50 ms of swing phase for the "no assist" condition for both the steady state and perturbed conditions.

We evaluated the effect of exoskeleton condition (no exo, no assist, eight conditions) on step placement outcomes in both steady state and perturbed trials using a one-way repeated measures analysis of variance (ANOVA). We used post-hoc comparisons with a Bonferroni correction to compare the no assist condition with the remaining nine conditions (no exo, eight assistance conditions). To evaluate the effect of the angle of the exoskeleton assistance vector relative to swing leg velocity on the change in step placement, we fit the data with a second-degree quadratic function and evaluated the p-value and R^2 of this fit. The threshold for significance was set at $\alpha = 0.05$.

IV. Results & Discussion

We first evaluated the influence of each exoskeleton condition on step placement (Fig. 6). During steady state and perturbed walking, the exoskeleton condition had a significant effect on both step width and length ($p < 0.001$ for all). We also evaluated how each condition (no exo, eight assistance conditions) compared to the no assist condition. In steady state walking, we detected significant differences ($p < 0.001$) in step width for all conditions except for the lengthening and shortening conditions and in step length for all conditions except for the narrowing conditions. In perturbed walking, we detected significant differences ($p < 0.001$) in step width for the widening, widening/lengthening, lengthening, narrowing, and narrowing/shortening conditions. For step length, we detected significant differences ($p < 0.001$) for the widening, widening/lengthening, lengthening, and narrowing/lengthening conditions. Across step width and length in the steady state and perturbed conditions, we found no significant differences between the no exo and no assist conditions. Generally, the exoskeleton was able to successfully deviate step width and length in both steady state and perturbed walking, with greater deviations in the former. We suggest that this may be due to the increased "risk" of incorrect step placement in perturbed situations where the individual is losing balance, causing them to somewhat resist the exoskeleton assistance in directions that may further worsen their balance.

An additional key finding is that there were no differences in step width or length due to wearing the exoskeleton with only gravity compensation assistance relative to not wearing

Authorized licensed use limited to: Georgia Institute of Technology. Downloaded on January 06,2025 at 23:11:39 UTC from IEEE Xplore. Restrictions apply.

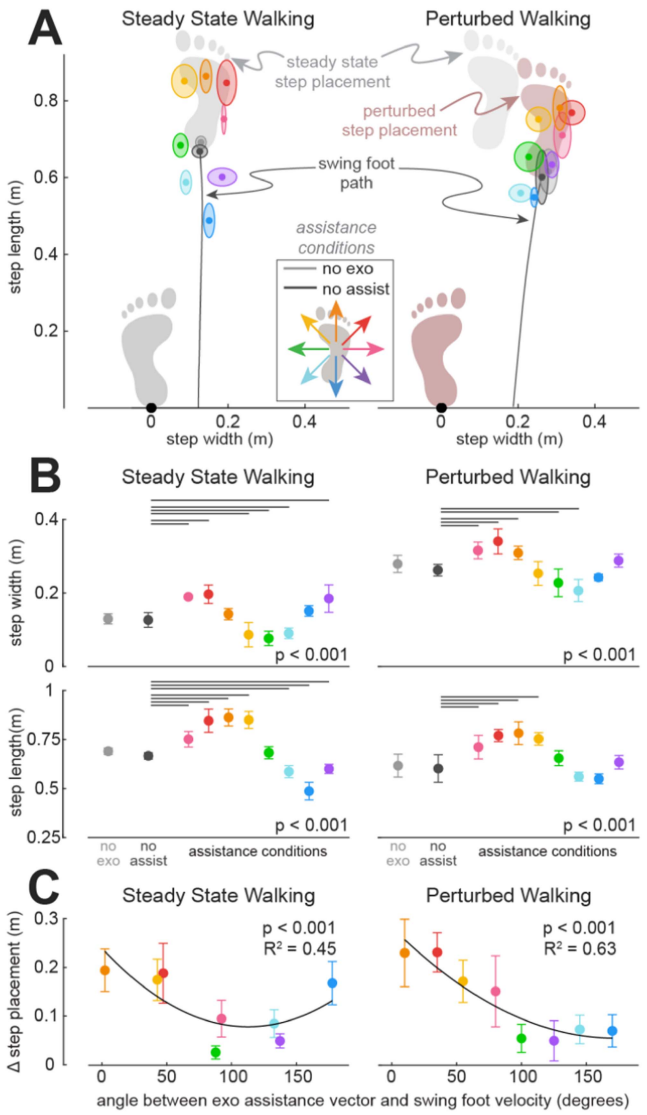

Fig. 6. (a) Bird's-eye view simultaneously shows the step width and length changes for each exoskeleton condition. Shaded ovals show ± 1 standard deviation. The mean swing foot path for the no assist condition is shown in dark grey. (b) The mean and ± 1 standard deviation are shown for step width and length. Resulting p-values from one-way ANOVA tests are shown and comparison bars indicate significant differences detected between the no assist condition and the remaining nine conditions. The threshold for significance was set at $\alpha = 0.05$. (c) The mean and ± 1 standard deviation are shown for each condition relative to that condition's assistance vector relative to the swing foot path and how that affects the change in step placement relative to the no assist condition. The best fit second-degree quadratic line and corresponding statistics are shown.

the exoskeleton. This supports the exoskeleton design and implementation presented in this work, as this lack of differences implies that we are not changing the participant's usual gait kinematics as a result of simply wearing the device.

Next, we evaluated how the angle of the exoskeleton assistance vector relative to swing leg velocity influenced the magnitude of step placement deviation. We expected that it would be easier to change step placement along the path of the swing leg, in comparison to changing placement perpendicular to the swing path. Specifically, we expected that there would be a bias towards conditions where the assistance vector aligned with the swing foot velocity, supported by previous work showing preference for positive power contributions from an exoskeleton [27]. Additionally, individuals tend to more tightly regulate mediolateral foot placement, compared to anteroposterior, and thus may resist assistance that tries to alter their typical mediolateral placement [12], [28]. Thus, we would expect larger step placement changes when the angle between the swing foot vector and exo assistance vector is near 0° and 180°, with a bias toward 0°, as well as smaller step placement changes in the middle of this range. We evaluated this by analyzing a second-degree quadratic best fit line; this fit was significant ($p < 0.001$) and showed moderate to strong correlations, with $R^2 = 0.45$ and $R^2 = 0.63$ for the steady state and perturbed conditions, respectively.

These results generally support our predictions that influencing step placement along the foot swing path is more feasible than perpendicular to this path. In the steady state condition, the step placement changes with and against the swing foot velocity vector were comparable, with slightly greater changes in conditions that aligned with the swing foot path, resulting in prominent step length changes. However, there was far less mediolateral deviation in step placement, which would be expected in the assistance conditions that cause deviations perpendicular to the swing foot path.

These findings vary a bit in the perturbed condition. The trend across different angles is generally the same, but with far less step placement deviation for the assistance conditions that opposed the foot swing path. We believe that this may be due to which assistance conditions were likely to aid in balance recovery. Generally, the perturbation condition induces COM velocity forward and toward the swing limb, requiring a longer and wider step to dissipate the perturbation's effects. As seen in Fig. 6(a), the unassisted step placement (shown by the footprint) is wider but shorter, not longer, which previous work suggests is due to the forward pitch shortening swing phase, which prevents further forward swing foot placement [12]. Because of this temporal limitation, it is likely that exoskeleton assistance that lengthens the swing foot path would be beneficial to users' balance recovery. We believe that this may be the reason that assistance in lengthening, and somewhat widening, directions were more effective, as the user may be more likely to allow, rather than resist, assistance if the exoskeleton is augmenting their inherent balance response.

There are limitations of this work that should be considered. The single participant and perturbation condition are meant to demonstrate initial promise of the device but prevent us from making broad conclusions about the exoskeleton's capabilities across diverse conditions. Additionally, the single participant inhibited our ability to randomize the order of perturbed and steady state sections of the experiment across a broader participant pool, which may have allowed adaptation to influence these results. Future studies that build on this preliminary work should consider expanding participant count, diversifying perturbation conditions, and designing protocols that account for possible adaptation throughout the study.

Broadly, this preliminary experimental verification supports our exoskeleton's ability to modulate step placement in both steady state and perturbed contexts. The findings suggest that human volition still plays a role in how the exoskeleton is able to modulate step placement, as expected with a device that is meant to have shared control with the user. Specifically, the perturbed condition suggests that individuals may resist less when

Authorized licensed use limited to: Georgia Institute of Technology. Downloaded on January 06,2025 at 23:11:39 UTC from IEEE Xplore. Restrictions apply.

the exoskeleton is contributing to balance recovery. Our future work will further explore the exoskeleton's capabilities across a variety of destabilizing contexts and investigate additional control approaches for balance augmentation.

ACKNOWLEDGMENT

The authors would like to thank Dr. Pawel Golyski, Dr. Inseung Kang, and Dr. Anirban Mazumdar for their input on mechanical design, as well as Reese Peterson, Sidd Nathella, Christoph Nuesslein, and Chris Meier for their input on mechatronic development.

REFERENCES

[1] A. D. Kuo and J. M. Donelan, "Dynamic principles of gait and their clinical implications," *Phys. Ther.*, vol. 90, no. 2, pp. 157–174, Feb. 2010.

[2] M. Arvin, M. J. M. Hoozemans, M. Pijnappels, J. Duysens, S. M. Verschueren, and J. H. van Dieën, "Where to step? Contributions of stance leg muscle spindle afference to planning of mediolateral foot placement for balance control in young and old adults," *Front. Physiol.*, vol. 9, Aug. 2018, Art. no. 1134.

[3] W. P. Berg, H. M. Alessio, E. M. Mills, and C. Tong, "Circumstances and consequences of falls in independent community-dwelling older adults," *Age Ageing*, vol. 26, no. 4, pp. 261–268, 1997.

[4] T. Zhang, M. Tran, and H. Huang, "Design and experimental verification of hip exoskeleton with balance capacities for walking assistance," *IEEE/ASME Trans. Mechatronics*, vol. 23, no. 1, pp. 274–285, Feb. 2018.

[5] V. Monaco et al., "An ecologically-controlled exoskeleton can improve balance recovery after slippage," *Sci. Rep.*, vol. 7, no. 1, Sep. 2017, Art. no. 46721.

[6] M. Afschrift et al., "Assisting walking balance using a bio-inspired exoskeleton controller," *J. NeuroEngineering Rehabil.*, vol. 20, no. 1, Jun. 2023, Art. no. 82.

[7] A. Alili, A. Fleming, V. Nalam, M. Liu, J. Dean, and H. Huang, "Abduction/adduction assistance from powered hip exoskeleton enables modulation of user step width during walking," *IEEE Trans. Biomed. Eng.*, vol. 71, no. 1, pp. 334–342, Jan. 2024.

[8] B. T. Sterke, K. L. Poggensee, G. M. Ribbers, D. Lemus, and H. Vallery, "Light-weight wearable gyroscopic actuators can modulate balance performance and gait characteristics: A proof-of-concept study," *Healthcare*, vol. 11, no. 21, Jan. 2023, Art. no. 2841.

[9] V. L. Chiu, M. Raitor, and S. H. Collins, "Design of a hip exoskeleton with actuation in frontal and sagittal planes," *IEEE Trans. Med. Robot. Bionics*, vol. 3, no. 3, pp. 773–782, Aug. 2021.

[10] S. Wang et al., "Design and control of the MINDWALKER exoskeleton," *IEEE Trans. Neural Syst. Rehabil. Eng.*, vol. 23, no. 2, pp. 277–286, Mar. 2015.

[11] H. Reimann, T. D. Fettrow, E. D. Thompson, P. Agada, B. J. McFadyen, and J. J. Jeka, "Complementary mechanisms for upright balance during walking," *PLoS One*, vol. 12, no. 2, Feb. 2017, Art. no. e0172215.

[12] J. K. Leestma, P. R. Golyski, C. R. Smith, G. S. Sawicki, and A. J. Young, "Linking whole-body angular momentum and step placement during perturbed walking," *J. Exp. Biol.*, vol. 226, no. 6, 2023, Art. no. jeb244760.

[13] A. L. Hof, S. M. Vermerris, and W. A. Gjaltema, "Balance responses to lateral perturbations in human treadmill walking," *J. Exp. Biol.*, vol. 213, no. 15, pp. 2655–2664, Aug. 2010.

[14] I. Kang, R. R. Peterson, K. R. Herrin, A. Mazumdar, and A. J. Young, "Design and validation of a torque-controllable series elastic actuator-based hip exoskeleton for dynamic locomotion," *J. Mechanisms Robot.*, vol. 15, Jun. 2022, Art. no. 021007.

[15] C. J. Arellano, D. P. O'Connor, C. Layne, and M. J. Kurz, "The independent effect of added mass on the stability of the sagittal plane leg kinematics during steady-state human walking," *J. Exp. Biol.*, vol. 212, no. 12, pp. 1965–1970, Jun. 2009.

[16] H. Herr and M. Popovic, "Angular momentum in human walking," *J. Exp. Biol.*, vol. 211, no. 4, pp. 467–481, Feb. 2008.

[17] S. W. John, K. Murakami, M. Komatsu, and S. Adachi, "Cross-wire assist suit concept, for mobile and lightweight multiple degree of freedom hip assistance," in *Proc. Int. Conf. Rehabil. Robot.*, 2017, pp. 387–393.

[18] S. H. Collins, P. G. Adamczyk, and A. D. Kuo, "Dynamic arm swinging in human walking," *Proc.. Biol. Sci.*, vol. 276, no. 1673, pp. 3679–3688, Oct. 2009.

[19] H. Gholizadeh, A. Hill, and J. Nantel, "Effect of arm motion on postural stability when recovering from a slip perturbation | Elsevier enhanced reader," *J. Biomech.*, vol. 95, 2019, Art. no. 109269.

[20] C. C. Gordon et al., "2012 anthropometric survey of U.S. army personnel: Methods and summary statistics," U.S. Army Natick Soldier Research and Engineering Center, Natick, Tech. Rep. Natick/TR-15/007, May 2014.

[21] J. Camargo, A. Ramanathan, W. Flanagan, and A. Young, "A comprehensive, open-source dataset of lower limb biomechanics in multiple conditions of stairs, ramps, and level-ground ambulation and transitions," *J. Biomech.*, vol. 119, Apr. 2021, Art. no. 110320.

[22] C. Nesler, G. Thomas, N. Divekar, E. J. Rouse, and R. D. Gregg, "Enhancing voluntary motion with modular, backdrivable, powered hip and knee orthoses," *IEEE Robot. Automat. Lett.*, vol. 7, no. 3, pp. 6155–6162, Jul. 2022.

[23] I. Kang, H. Hsu, and A. Young, "The effect of hip assistance levels on human energetic cost using robotic hip exoskeletons," *IEEE Robot. Automat. Lett.*, vol. 4, no. 2, pp. 430–437, Apr. 2019.

[24] J. K. Leestma, P. R. Golyski, C. R. Smith, G. S. Sawicki, and A. Young, "Biomechanics of locomotion during ground translation perturbations," Georgia Institute of Technology, Mar. 2023.

[25] S. Alazzawi, M. H. Field, N. V. Bardakos, M. A. R. Freeman, and R. E. Field, "The position of the centre of the femoral head relative to the midline of the pelvis: A consistent landmark in total knee replacement surgery," *Knee*, vol. 19, no. 6, pp. 827–831, Dec. 2012.

[26] A. Leardini et al., "Validation of a functional method for the estimation of hip joint centre location," *J. Biomech.*, vol. 32, no. 1, pp. 99–103, Jan. 1999.

[27] Y. Ding et al., "Effect of timing of hip extension assistance during loaded walking with a soft exosuit," *J. NeuroEngineering Rehabil.*, vol. 13, no. 1, Oct. 2016, Art. no. 87.

[28] Y. Wang and M. Srinivasan, "Stepping in the direction of the fall: The next foot placement can be predicted from current upper body state in steady-state walking," *Biol. Lett.*, vol. 10, no. 9, Sep. 2014, Art. no. 20140405.

Authorized licensed use limited to: Georgia Institute of Technology. Downloaded on January 06,2025 at 23:11:39 UTC from IEEE Xplore. Restrictions apply.